analytical chemistry

pubs.acs.org/ac Article

Addressing Buffer, Size, and Clogging Challenges in LAMP-Coupled Solid-State Nanopores for Point-of-Care Testing

Ming Dong, Aneesh Kshirsagar, Anthony J. Politza, Muhammad Asad Ullah Khalid, Md Ahasan Ahamed, and Weihua Guan*

Cite This: *Anal. Chem.* 2025, 97, 7879−7887 Read Online

ACCESS | Metrics & More | Article Recommendations

ABSTRACT: Loop-mediated isothermal amplification (LAMP) is a promising method for point-of-care nucleic acid testing due to its simplicity, rapidity, and high sensitivity. Coupling LAMP with solid-state nanopores enables label-free, single-molecule sensing, enhancing diagnostic accuracy. However, conventional LAMP-coupled nanopore protocols require high-salt buffers (>1 M) to improve signal strength and translocation frequency, complicating workflows and increasing contamination risks. In native LAMP buffers (50 mM KCl), electroosmotic flow (EOF) hinders amplicon transport in sub-10 nm pores, while large amplicons increase the risk of clogging. These challenges limit event rates, data throughput, and device reliability. To address these limitations, we developed a glass nanopore device optimized for direct sensing of amplicons in native buffers, featuring integrated declogging capabilities. Our results revealed that 200 nm pores provided the best balance between minimizing EOF interference and maintaining strong signal strength, achieving the highest event rates. Smaller pores (<100 nm) had low event rates due to EOF effects, while larger pores (>1 μm) showed weakened signal strength. We discovered that clogging in low-salt conditions differs from high-salt environments, with physical vibration effectively resolving clogging in low-salt settings. This led to the integration of an automated vibration motor, extending nanopore lifespan and ensuring continuous data acquisition. Our clog-free, native-buffer sensing platform demonstrated a sensitivity of 0.12 parasite/μL using *Plasmodium vivax* (*P. vivax*) as a model organism, exceeding the threshold for detecting asymptomatic infections. These advancements highlight the potential of our nanopore device for rapid, reliable, and user-friendly diagnostics for point-of-care testing.

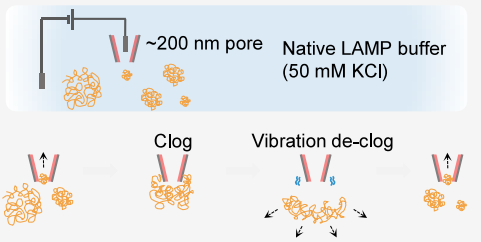

Loop-mediated isothermal amplification (LAMP) is highly suited for point-of-care nucleic acid testing due to its simplicity, rapidity, and sensitivity, which address critical challenges in decentralized diagnostics.[1,2] Unlike traditional polymerase chain reaction (PCR), LAMP operates under isothermal conditions, typically at 60−65 °C, eliminating the need for complex thermal cycling equipment. This significantly reduces the cost, energy requirements, and operational complexity, making it ideal for resource-limited or field settings. The LAMP assay can be coupled with various detection methods, such as colorimetric, turbidimetric, fluorescence, or nanopore-based readouts, providing flexibility for integration into portable diagnostic devices. While methods like colorimetric and turbidimetric detection are simple and cost-effective, they often lack the sensitivity and specificity required for detecting low-abundance targets.[3,4] Fluorescence-based LAMP assays offer higher sensitivity and can be quantitative when combined with real-time monitoring. However, they require fluorescent dyes or probes, specialized optical equipment, and are susceptible to photobleaching and background fluorescence interference.[5] Among those methods, LAMP-coupled nanopore testing stands out for its label-free, single molecular level sensing mechanism.[6−9] Additionally, the ability to size-discriminate LAMP amplicons using nanopores potentially promotes another layer of specificity that further enhances diagnostic accuracy. Compared to biological nanopores, solid-state nanopores offer superior mechanical robustness, chemical stability, and can operate under varying pH, temperature, and ionic strength conditions.[10−13] These attributes make solid-state nanopores suited for integration into portable diagnostic devices, which can be used in diverse environments and resource-limited locations.

While LAMP-coupled nanopore sensing has demonstrated high specificity and sensitivity, several challenges must be addressed before this platform can be effectively promoted for portable diagnostic devices.[14−16] First, most LAMP-coupled nanopore sensing protocols require the addition of over 1 M salt to enhance signal strength and translocation frequency.[17] However, this step complicates the process and increases contamination risks, making native LAMP buffers (50 mM

Received: December 16, 2024
Revised: March 4, 2025
Accepted: March 5, 2025
Published: March 11, 2025

https://doi.org/10.1021/acs.analchem.4c06823
Anal. Chem. 2025, 97, 7879−7887

KCl) a safer and more user-friendly option for portable devices. Additionally, high-salt conditions eliminate the possibility of monitoring the amplification process in real-time. Sensing in low-salt native buffers, however, presents challenges, as electroosmotic flow (EOF), arising from electrostatic interactions in the electric double layer (EDL), can hinder amplicon translocation.[18,19] In sub-10 nm nanopores, the competing forces between electrophoresis (EP) and EOF reduce translocation rates, resulting in low event frequency and limited data throughput.[17] Second, unlike PCR amplicons, LAMP amplicons vary significantly in size, ranging from a few hundred base pairs to hundreds of kilobases, posing challenges for effective nanopore-based detection.[14,20] The high concentration and large size of amplicons increase the likelihood of interactions with pore walls, often leading to partial or complete clogging, which disrupts event rate determination and shortens nanopore lifespan.[14,16,21−23] While voltage cycling has been proposed to address clogging, permanent clogs can still occur, especially in low-salt native buffers where reduced electrophoretic forces further hinder declogging.[14,16] Larger nanopores are expected to mitigate clogging by allowing bulky amplicons to translocate in a recoiled state rather than threading through sub-10 nm pores. We hypothesize that LAMP amplicons can be effectively detected using larger pores in native buffers (50 mM KCl) due to reduced surface effects and compatibility with amplicon size. However, capturing amplicon signals in low-salt conditions remains challenging due to reduced capture efficiency and signal intensity. Therefore, a reliable nanopore device with an optimal pore size and integrated declogging functionality is essential for continuous, effective LAMP amplicon detection in native buffers.

In this study, we developed a glass nanopore device capable of directly sensing amplicons from LAMP native buffer, featuring integrated declogging capabilities and optimized size for qualitative LAMP assay readouts. Unlike traditional nanopore-based LAMP sensing, which typically operates in high-salt conditions and frequently encounters clogging, our approach enables clog-free amplicon detection in native low-salt buffers, simplifying sample preparation and reducing contamination risks. We observed that pores smaller than 100 nm had low event rates due to EOF interference, while pores larger than 1 μm showed reduced event rates due to weakened signal strength. In contrast, 200 nm pores effectively detected LAMP amplicons in low-salt conditions with minimal EOF interference, reaching the optimal balance between reducing EOF impedance and maintaining strong signal strength, leading to the highest event rate. We discovered that the clogging behavior in low-salt environments differs from the jamming in high-salt conditions, and simple physical vibration can effectively resolve clogging in low-salt settings. This led to the development of a customized nanopore holder with an integrated vibration motor, extending pore lifespan and enabling continuous data acquisition. We further implemented automated declogging to improve the reliability of nanopore-based LAMP assay readouts. At an estimated cost of $7 per device, it offers cost-efficiency with the potential for miniaturization and integration into portable devices. The device could be scaled for large-volume production with advances in microfabrication and automation. These advancements in clog-free amplicon sensing in native buffer conditions demonstrate the platform's potential for clinical and field applications, providing a reliable, rapid, and user-friendly solution.

EXPERIMENTAL SECTION

Materials and Chemicals. Quartz capillaries (QF100-50-7.5) with inner and outer diameters of 0.5 and 1 mm were used in our experiment (Sutter Instrument). Ag/AgCl electrodes were homemade with 0.2 mm Ag wires (Warner Instruments). The microinjector (MF34G-5) with 34 gauge was purchased from World Precision Instruments. KCl (L9650) and Tris-EDTA buffer solution (pH 8.0, 93283) were purchased from Sigma-Aldrich. The KCl solution was filtered with a 0.2 μm syringe filter (WHA67802502, Whatman). The malaria *Plasmodium vivax* (*Pv.*) genomic DNAs (5 ng/μL) were gifts from Dr. Cui's lab at Penn State, extracted by the phenol-chloroform-based procedure. *Bst* 2.0 DNA polymerase (M0537), nuclease-free water (B1500), isothermal amplification buffer (B0537), deoxynucleotide solution mix (N0447), magnesium sulfate solution (B1003) were purchased from New England Biolabs.

Glass Nanopore Fabrication. The quartz capillaries were initially cleaned with piranha solution (H_2SO_4: H_2O_2 at a 3:1 ratio) at 95 °C for 30 min to remove organic contaminants. They were then thoroughly rinsed with deionized water and dried in an oven at 100 °C for 15 min. A laser pipet puller (P-2000, Sutter Instruments) was used to fabricate the nanopore using a two-line program: (1) Heat 575, Filament 3, Velocity 35, Delay 145, and Pull 75; (2) Heat 435, Filament 0, Velocity 15, Delay 128, and Pull 185. This standard recipe generally yields a nanopore size of approximately 200 nm. Adjustments were made to the Heat and Pull settings in the second line to fabricate nanopores of various sizes, facilitating the exploration of size-dependent amplicon counting.

Nanopore Device Assembly and Measurement. The PMMA tube (inner diameter 4 mm, outer diameter 5 mm) was purchased from MECCANIXITY, and the PMMA sheets with a thickness of 3/16-in. were purchased from ePlastics. These sheets were shaped using a laser cutter and assembled using IPS Weld-On 3 adhesives. Additionally, a PDMS O-ring was created using the SYLGARD 182 Silicone Elastomer kit, by mixing the elastomer and curing agent in a 10:1 weight-to-weight ratio. The DC vibration motor (Part # 5101-JYZ0612WP-ND, ERM 15000 rpm, 3 V DC, 6 mm Dia, 10.79 mN·m) was attached to the holder with Epoxy adhesive (3 M Scotch-Weld DP100). The whole device is made from primary materials including a glass nanopore (~$2), PMMA nanopore holder (~$3), and a vibration motor (~$2), bringing the estimated total cost per device to around $7. Attempts to fill glass pores directly with isothermal amplification buffer were made, but this often resulted in bubble formation inside the glass pipet, preventing the tip from becoming fully wetted. The fabricated nanopore is loaded with 50 mM KCl using a microinjector to create a symmetric salt condition with the sample's native LAMP buffer. The glass pores are initially placed into the PDMS O-ring within the PMMA tube shell. Subsequently, the tube containing the glass nanopore is inserted into the PMMA holder, and the sensing electrode is simultaneously inserted into the glass nanopore. A 400 mV voltage bias was applied to the nanopore using a 6363 DAQ card (National Instruments) during sensing experiments. Ionic current recordings were captured by an Axopatch 200B amplifier (Molecular Device). These recordings were digitized using the same DAQ card, processed through a custom

https://doi.org/10.1021/acs.analchem.4c06823
Anal. Chem. 2025, 97, 7879−7887

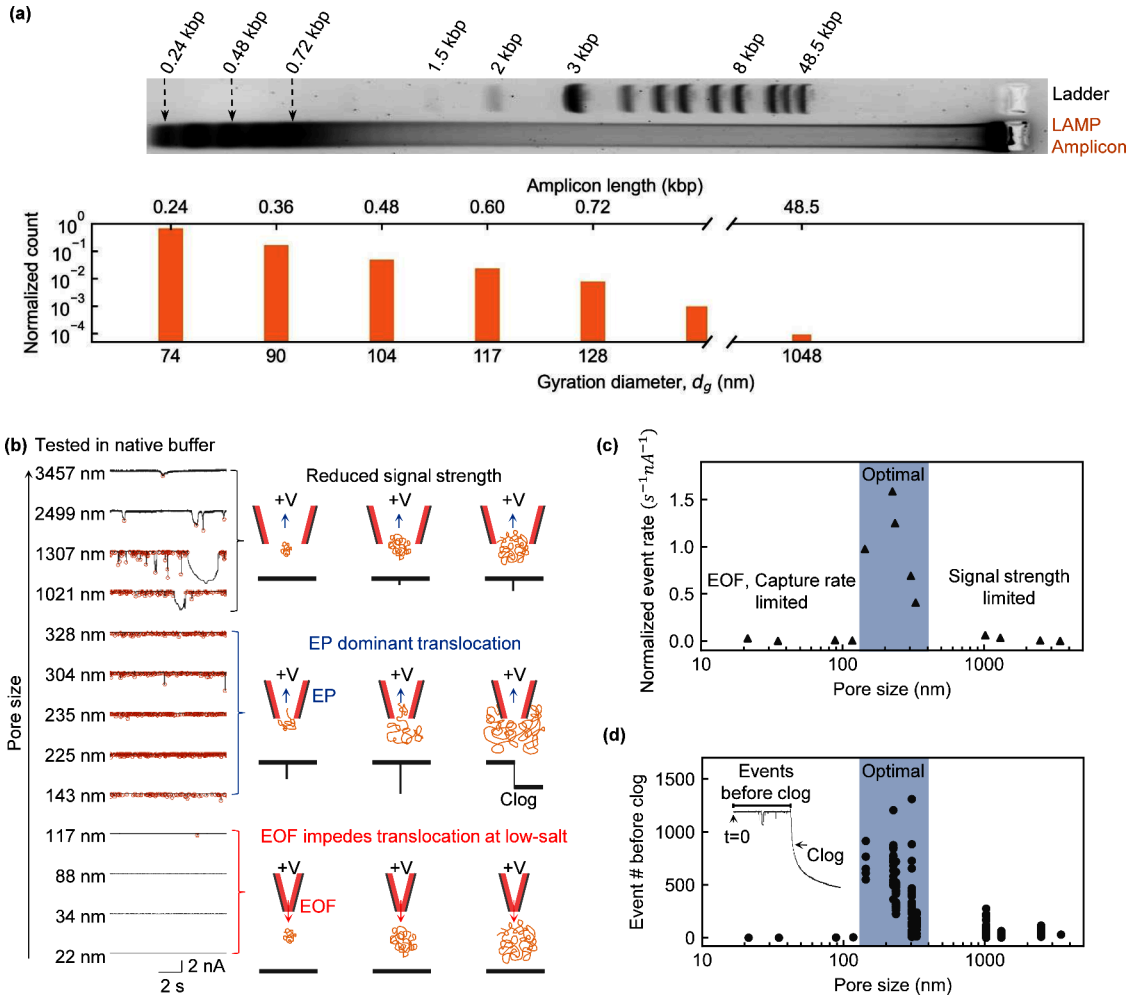

Figure 1. Counting behavior of LAMP amplicons in native buffer with different sized nanopores and clogging characteristics. (a) Gel image depicting the amplicon length, and the corresponding distribution based on different gyration diameters. (b) Current traces from 13 nanopores sensing the same LAMP positive sample, along with schematics illustrating the nanopore counting behavior at various sizes. The red region represents the EDL. (c) Correlation between normalized event rate (Event rate R (s^{-1}) normalized by baseline current I_b (nA)) and nanopore size. (d) Correlation between the number of events before clogging and pore size.

LabVIEW program at a sampling frequency of 100 kHz, and subjected to a 10 kHz low-pass filter. The vibration motor was controlled by the DAQ card. The nanopore measurement setup was housed within a custom-made Faraday cage to minimize environmental electrical noise, and prevent aerosol contamination from affecting the nanopore readings.

LAMP Assay. The total volume of the LAMP assays contains a 24 μL master mix and 1 μL Malaria *P. vivax* gDNA (For the no template control (NTC), 1 μL of nuclease-free water was used as a replacement). The Malaria *P. vivax* gDNA, provided by Dr. Cui's lab at Penn State, had a stock concentration of 5 ng/μL. This gDNA was then serially diluted down to concentration of 0.005 fg/μL. The master mix includes isothermal buffer (20 mM Tris−HCl, 10 mM $(NH_4)_2SO_4$, 50 mM KCl, 2 mM $MgSO_4$, 0.1% Tween 20), nuclease-free H_2O, $MgSO_4$ (7 mM), SYTO-9 green (5 μM), deoxyribonucleotide triphosphates (dNTPs, 1.4 mM), Bst 2.0 DNA polymerase (0.4 U/μL), primer sets (0.2 mM F3 and B3c, 1.6 mM FIP and BIP, 0.8 mM LF and LB). The reaction was performed at a constant temperature of 65 °C for 10 min using a benchtop PCR instrument (Bio-Rad CFX96).

RESULTS AND DISCUSSION

Pore Size-Dependent LAMP Amplicon Counting in Native Buffer. During the LAMP reaction, DNA targets were amplified through a series of strand displacement and extension reactions, generating amplicons of varying lengths. These amplicons can range from a few hundred base pairs to hundreds of kilobases, and the population of amplicons typically follows a distribution where shorter fragments are present in higher numbers due to their faster amplification kinetics.[14,20] To investigate the feasibility of detecting LAMP amplicons in native buffer conditions, and determine the optimal pore size for LAMP amplicon sensing, we conducted experiments using pores of various sizes. In Figure 1a, the gel image of LAMP amplicons from positive samples shows their lengths ranging from hundred base pairs to over 48.5 thousand base pairs. Applying the gyration radius formula, the estimated gyration diameter of these amplicons spans from 74 nm to more than 1048 nm.[24] Consequently, we hypothesize that pores in the micrometer range could still effectively detect LAMP amplicons due to their comparable dimensions. Figure 1b left panel shows the current traces of 13 different nanopores with sizes ranging from 22 to 3457 nm. It should be noted that

https://doi.org/10.1021/acs.analchem.4c06823
Anal. Chem. 2025, 97, 7879−7887

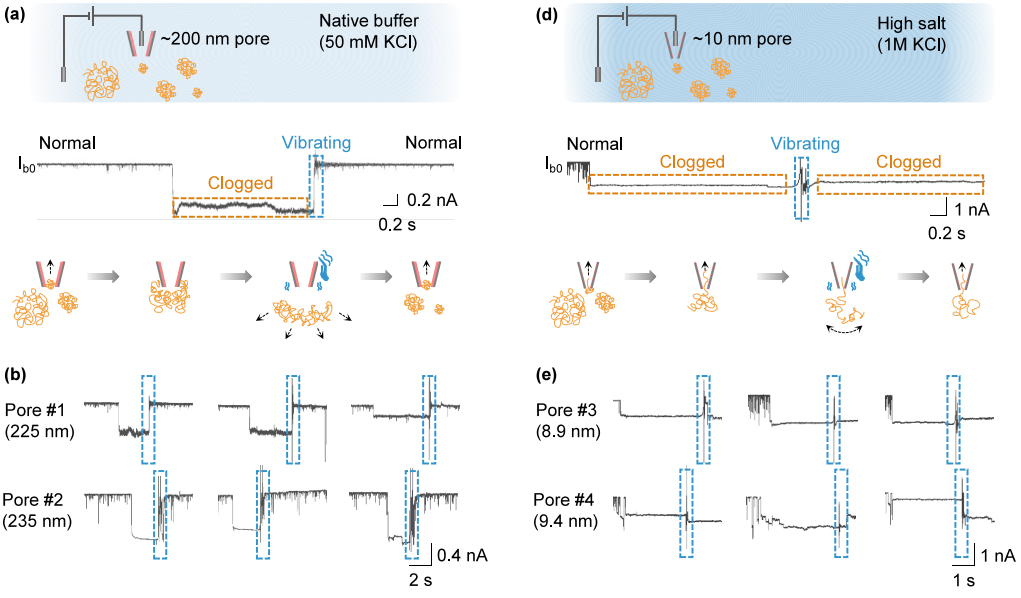

(c)

Pore size	Average clogging level	De-clogging by manual vibrating	Successful de-clog rate
225 nm	0.93 I_{b0}	19/19	100%
235 nm	0.91 I_{b0}	28/28	100%

(f)

Pore size	Average clogging level	De-clogging by manual vibrating	Successful de-clog rate
8.9 nm	0.78 I_{b0}	5/49	10%
9.4 nm	0.84 I_{b0}	6/47	13%

Figure 2. Vibrating-assisted declogging of pores in native and high-salt buffer conditions. (a) Schematic illustrating LAMP amplicon sensing with a 200 nm pore in native buffer. The representative current trace shows normal counting, clogging, declogging by manual vibration, and a return to normal counting. (b) Representative current traces from two different-sized pores demonstrate successful declogging. (c) Summary table of clogging and declogging statistics for 25× diluted LAMP amplicons measured with two pores at native buffer. (d) Schematic of LAMP amplicon sensing with a 10 nm pore in 1 M KCl buffer. The current trace shows normal counting, clogging, an attempt to declog with manual vibration, and the pore remaining clogged. (e) Representative current traces from two different-sized pores show ineffective declogging. (f) Summary table of clogging and declogging statistics for 25× diluted LAMP amplicons measured with two pores at high salt.

events with more than 1 s dwell time are treated as temporary clogging of nanopores since the dwell time of amplicon translocation is typically under a millisecond scale. Therefore, those long dwell time blockages are excluded to avoid introducing noise to the nanopore counting result. Figure 1b right panel illustrates the hypothesized counting behaviors for nanopores of various sizes in relation to different-sized amplicons. When the pore size is relatively small (under 100 nm), the interplay between electrophoresis and electroosmotic flow may impede the translocation of negatively charged LAMP amplicons through the nanopore at low-salt concentrations.[17] As pore sizes increase, the influence of the EDL on amplicon translocation diminishes, given that the EDL thickness is typically less than 10 nm in a 50 mM KCl solution.[25,26] In this scenario, electrophoresis emerges as the dominant force, leading to an increase in the event rate. However, as the pore size reaches the micrometer range, the ability to detect shorter LAMP amplicons via the blockage current signal becomes less pronounced, decreasing the event rate.

To identify the optimal pore size for LAMP amplicon sensing in the native buffer, we investigated the counting behaviors of those various nanopores. Previous work has demonstrated that the event rate increases linearly with the baseline current value.[27] Therefore, we used a normalized event rate relative to the baseline current values, to assess each pore's ability to detect amplicons in the native buffer. The capture rate of molecules can be represented by the equation: $R = \frac{\mu N_A C_{mol}}{\Lambda C_{ion}} I_b$, where C_{mol} is the molecule concentration, and I_b is the pore baseline current value.[17] Thus, the normalized event rate (R/I_b) can also represent the effective molecule concentration that is detectable by the pores. To minimize the impact of reaction time on amplicon size variation and ensure consistent results, we standardized the LAMP reaction time to 70 min. The correlation between the normalized event rate and pore size, depicted in Figure 1c, shows that the event rate first increases and then decreases as pore size grows, aligning with the hypothesis illustrated in Figure 1b. Similarly, the number of capture events before the clogging, as shown in 1d, follows the same pattern, which increasing at first and then decreasing with larger pore sizes. This pattern can be attributed to the small capture radius at sub-100 nm pore sizes and reduced interactions between molecules and the pore walls as the pore size approaches the micrometer range. These observations suggest that, for maximizing data throughput in the native buffer sensing, a pore size ranging from 150 to 300 nm is optimal, as it yields the highest detectable amplicon concentration and the greatest number of events before clogging occurs.

Discovery of Vibrating-Assisted Nanopore Declogging. LAMP sensing involves large, recoiled amplicons that often clog nanopores due to their size and shape, disrupting the detection process. Methods like IV sweep or inverted bias

https://doi.org/10.1021/acs.analchem.4c06823
Anal. Chem. 2025, 97, 7879−7887

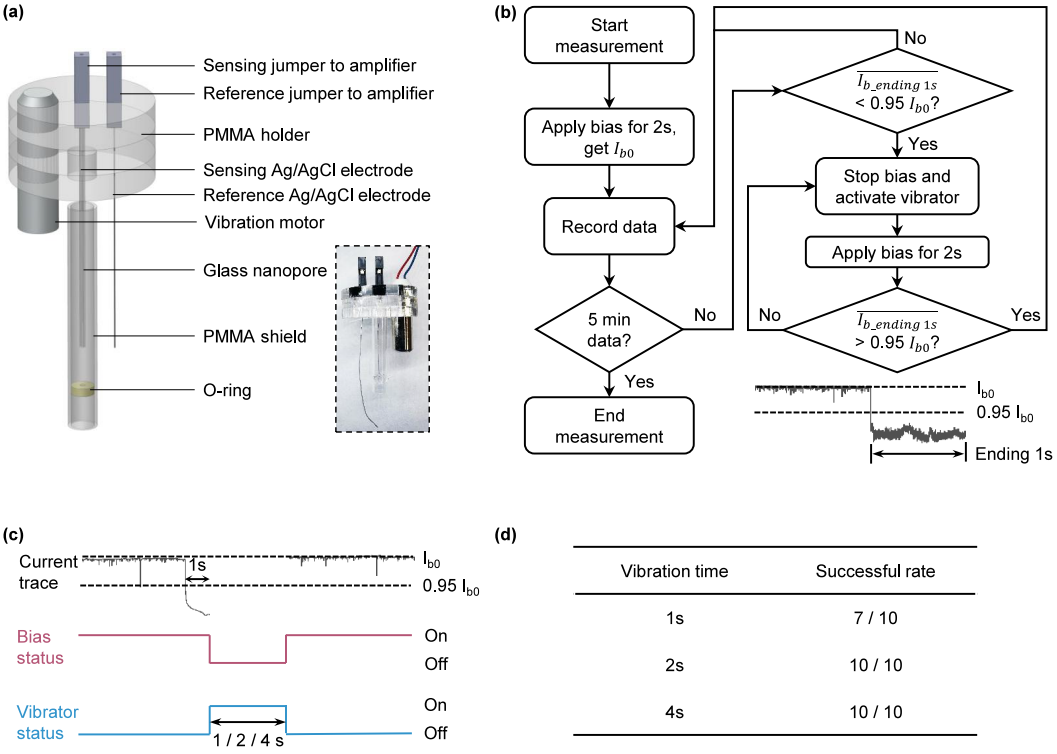

Vibration time	Successful rate
1s	7 / 10
2s	10 / 10
4s	10 / 10

Figure 3. Assembly, workflow, and performance evaluation of the automated declogging system. (a) Schematic illustration of the nanopore device assembly, highlighting key components. (b) Flowchart detailing the logic algorithm for glass nanopore measurements and the automated activation of the declogging process. (c) Timeline showing the bias and vibrator status during typical operations, emphasizing the intervals when the bias is paused for vibration-induced declogging. (d) Table summarizing the declogging success rates for various vibration durations. A clogging event resolved within five vibrations is deemed successful.

offer limited success, especially in low-salt native buffers.[14] We explored the clogging mechanisms and identified several contributing factors. First, high amplicon concentrations can lead to aggregation, forming complexes too large to pass through the pore.[28,29] Second, electrostatic and hydrophobic interactions cause amplicons to adhere to pore walls, narrowing the effective pore size.[30] Third, low-salt native buffers increase electroosmotic flow (EOF), which impedes amplicon translocation and enhances interactions with the nanopore walls due to reduced charge screening.[18,19,31] These factors highlight the need for a more effective declogging strategy to ensure reliable nanopore sensing in native buffer conditions.

Intriguingly, we found that manually vibrating the pore holder effectively cleared clogs, a finding with significant implications for nanopore sensing in low-salt native buffers. The manual vibration was applied by a single tap on the top of the nanopore holder, using a force similar to knocking on a door. As depicted in Figure 2a, normal event spikes appeared initially, but the pores soon clogged, likely due to large LAMP amplicons blocking the entrance, indicated by a drop in baseline current (I_{b0}). When clogging persisted for over one second, manual vibration introduced mechanical shaking, visible as vibrations in the current trace. This action successfully restored the baseline current to its open-pore value, allowing sensing to continue. This manual intervention utilizes vibration-induced hydraulic repulsion, where mechanical vibrations generate subtle fluid movements around the pore entrance.[32,33] While the nanoscale mechanisms behind clogging and vibration-induced declogging remain unexplored, future studies using fluorescent dyes could possibly track amplicon translocation and declogging dynamics in real time under a microscope.[34] In addition, atomic force microscopy and molecular dynamics simulations could also help to gain a deeper understanding of these declogging mechanisms.[35−37]

To validate the efficacy of manual vibrating in declogging, we carried out LAMP amplicon sensing experiments using different nanopore devices. As depicted in Figure 2b, we employed two nanopore devices with sizes of 225 and 235 nm, which are within the optimal size range for LAMP amplicon counting in the native buffer. We manually tapped the pore holder to induce vibrations whenever these pores experienced clogging for more than one second. The representative current traces from these devices demonstrate that manual vibrating can effectively restore the functionality of clogged pores without causing damage, as evidenced by the unchanged baseline current values postvibrating. Figure 2c presents the clogging and declogging statistics for the nanopore devices, showing that the average clogging level ranged from 91 to 93% of I_{b0}. Additionally, it demonstrates that manual vibrating resolved clogging events with a 100% success rate. This outcome suggests that vibration, induced through manual vibrating, could be a potent and reliable method for declogging pores, thereby maintaining continuous sensing. This declogging technique offers a noninvasive and instant method to restore nanopore functionality while preserving the structural integrity of the nanopore.

Building on the success of vibration-assisted declogging in low-salt setups, we examined its efficacy in a traditional high-salt (1 M KCl) environment using sub-10 nm nanopores. As shown in Figure 2d, in high-salt conditions, EOF is negligible due to the EDL thickness being less than 0.3 nm,[26] and strong

https://doi.org/10.1021/acs.analchem.4c06823
Anal. Chem. 2025, 97, 7879−7887

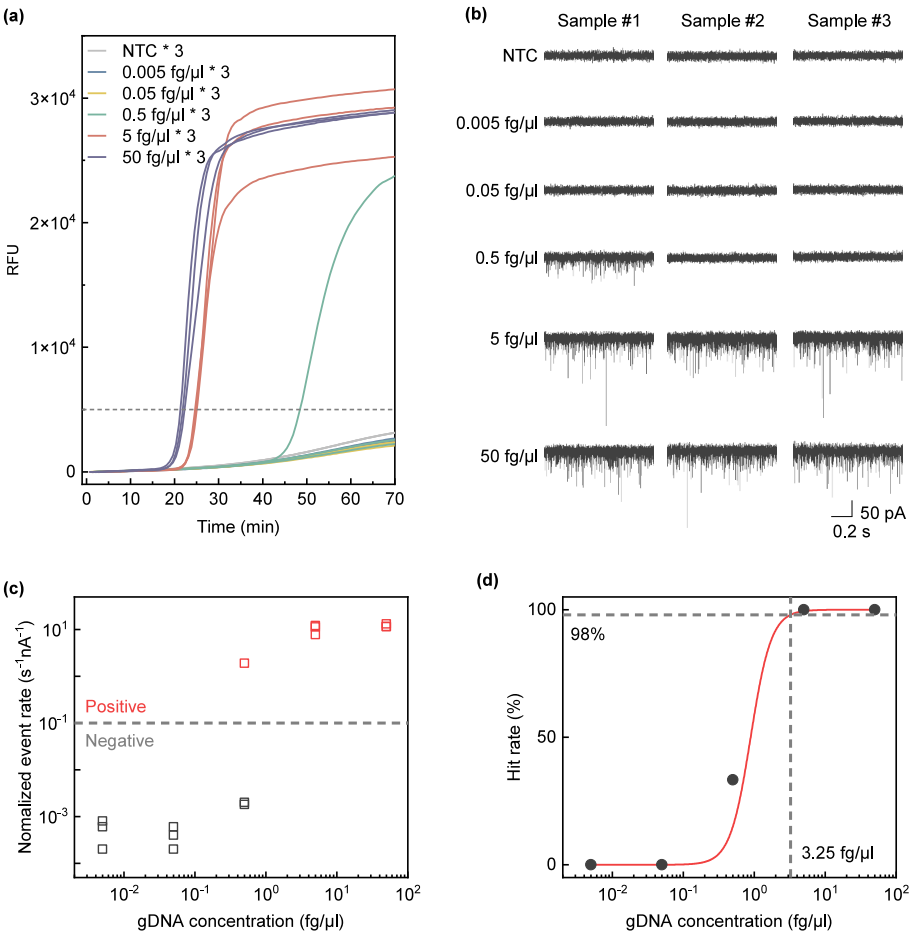

Figure 4. Analytical sensitivity evaluation of the native buffer LAMP sensing platform. (a) Real-time amplification curves and measurement setup. LAMP samples were prepared with varying concentrations of malaria *P. vivax* gDNA, with triplicate samples for each concentration. (b) Current traces from the nanopore sensing of LAMP samples containing different concentrations of malaria *P. vivax* gDNA. (c) The normalized event rate for the LAMP samples across different gDNA concentrations, employing a threshold of 0.1 s^{-1} nA^{-1} to differentiate between positive and negative results. (d) Hit rate data extracted at various gDNA concentrations to establish the limit of detection.

electrophoretic forces drive amplicons into the nanopore. As a result, the amplicons are tightly pulled into the 10 nm nanopore, causing more severe clogging compared to the low-salt, 200 nm pore configuration. When manual vibration was applied, the jammed amplicons could not be dislodged, leaving the nanopore clogged. In Figure 2e, the current traces from 8.9 and 9.4 nm pores, clearly show that manual vibration could not effectively restore the clogged nanopore, as indicated by the baseline current levels failed to return to the open-pore levels. The clogging statistics shown in Figure 2f further illustrate that the clogging severity is more significant in the high-salt setup, with clogging levels ranging from 78 to 84% of the I_{b0}. This highlights a critical difference between clogging mechanisms in low-salt environments and jamming in high-salt conditions. The increased electrophoretic forces and clogging severity in high-salt environments make manual vibration-assisted declogging far less effective. These findings underscore the potential of efficient vibration-assisted declogging in the low-salt, 200 nm pore configuration as a promising strategy for improving the reliability and usability of nanopore-based LAMP sensing systems in native buffer conditions. By mitigating clogging and ensuring continuous operation, this approach enhances the reliability and usability of nanopore-based LAMP sensing systems in native buffer conditions.

Integrated Nanopore Device with Automated Declogging. To address the challenge of nanopore clogging during LAMP amplicon sensing, we have implemented a vibration motor (15,000 rpm, 3 V DC) to facilitate automated declogging. This approach substitutes the manual vibration to dislodge clogged LAMP amplicons effectively with hydraulic repulsion.[32,33] Figure 3a presents a detailed schematic of the nanopore device assembly, highlighting the key components. We utilize a protective PMMA tube shield to protect the delicate glass nanopore tips. This shield protects against physical damage and contamination during handling and storage, maintaining the integrity and functionality of the nanopore. Dupont jumpers are used to simplify connections with the amplifier and DAQ system. An eccentric vibration motor is employed to induce vibrations to the nanopore device, aiming to facilitate the declogging of the nanopore. The assembled nanopore device can be easily inserted into a standard 200 μL centrifuge tube, commonly used in amplification assays, functioning similarly to a pH meter. This setup is engineered for seamless integration with standard nanopore laboratory equipment, ensuring robust operation.

The operational logic for current signal monitoring and automatic declogging is depicted in Figure 3b. The process begins by applying an electrical bias to establish a baseline current (I_{b0}) through the nanopore. Recognizing that most

https://doi.org/10.1021/acs.analchem.4c06823
Anal. Chem. 2025, 97, 7879−7887

clogs result in a current reduction to less than 95% of I_{b0} (as shown in Figure 2c), the system identifies a sustained drop to 95% of I_{b0} for more than one second as indicative of a clog. Upon detecting this, the system pauses the bias to the nanopore and activates the vibration motor. The bias is then reapplied to determine if the nanopore current has returned to normal levels, enabling the continuation of amplicon translocation data recording. This automated response is specifically designed to clear clogs without human intervention. Figure 3c presents a timeline of a typical sensing operation, including the intervals when the bias is active and when it is paused for declogging. If the current drops to 95% of I_{b0} for more than one second, the bias is turned off, and data acquisition is halted while the vibration motor is activated for a set duration. Afterward, the voltage bias is reapplied to assess the effectiveness of the declogging and to continue data acquisition. To evaluate the effectiveness of the automated vibration-assisted declogging, we conducted trials varying the duration of the vibrations. Figure 3d summarizes the results, indicating that vibrations lasting more than 2 s are generally effective in clearing nanopore clogs, thus minimizing downtime and potential data loss. Compared to manual vibrating, the integrated glass nanopore device also consistently achieved a 100% declogging rate with its automated system. By integrating a vibration motor into the LAMP sensing system, the operational lifespan of the glass nanopores is significantly extended, reducing both downtime and maintenance frequency. This automated declogging method enhances the durability of the nanopores, thus boosting the overall throughput and reliability of the sensing system. To evaluate the long-term stability of the device, further assessments could be conducted to ensure consistent performance over extended periods in native buffer conditions. These tests will focus on signal degradation, clogging frequency, and event rate consistency, while also considering the impact of repeated use, environmental factors, and storage conditions.

Sensitivity Validation Using Malaria LAMP Assay as a Model. After validating the automated declogging nanopore sensing platform, we assessed its sensitivity within the native buffer to determine if it meets the required sensitivity for early stage pathogen detection. We conducted LAMP assays for Malaria *P. vivax* by adding 1 μL of gDNA to the reaction master mix, with concentrations ranging from 0.005 to 50 fg/μL. We prepared triplicate samples for each concentration and conducted the LAMP reactions at 65 °C for 70 min (Figure 4a displays the real-time amplification curves obtained with Bio-Rad CFX96). Following the reaction, the samples were cooled to room temperature, and the 200 nm nanopore device was directly inserted into the 200 μL centrifuge tube containing 25 μL samples to begin the sensing experiment. Each sample was tested until 5 min of unclogged traces were recorded. Figure 4b displays the current traces obtained from sensing LAMP samples at varying gDNA concentrations. No detectable events were observed in the no-template control (NTC), indicating that the nanopore does not detect signals from the reagents alone. Figure 4c illustrates the normalized event rate across these concentrations, using a threshold of 0.1 s^{-1} nA^{-1} to distinguish between positive and negative results. At the tested concentration of 0.5 fg/μL, only one out of three samples showed a positive result, potentially due to the low amount of genome added into the assay. In contrast, all samples were positively identified at 5 and 50 fg/μL gDNA concentrations.

To determine the limit of detection (LoD) of our clog-free LAMP native buffer sensing platform, we analyzed the hit rates at various gDNA concentrations, where the hit rate is defined as the ratio of positive tests to total tests at a given concentration. As depicted in Figure 4d, the hit rate declines from 100 to 33% as the gDNA concentration decreases from 5 to 0.5 fg/μL. We applied a logistic curve to model the experimental hit rate data, establishing a LoD of approximately 3.25 fg/μL gDNA at a 98% confidence level. Given that the genome of the Malaria *P. vivax* parasite is approximately 27 Mbp, corresponding to 27.62 fg,[38] the sensitivity of our platform is estimated to be about 0.12 parasite/μL. According to the World Health Organization's guidelines for analytical sensitivity, detecting infections in asymptomatic individuals requires the capability of identifying at least 2 parasites/μL. Our platform's sensitivity successfully meets this criterion, underscoring its potential for early stage infection diagnostics and its effectiveness in identifying low-level infections. While we have demonstrated the sensitivity of the system using *P. vivax* as a model pathogen, further validation with additional pathogens would better showcase the versatility and robustness of the platform. This expanded validation would help assess its performance across different types of amplicons, reaction conditions, and pathogen genomes, and could provide valuable insights into the consistency of nanopore sensing for varied diagnostic targets. The development of this LAMP-coupled nanopore platform marks a significant advancement in delivering sensitive and qualitative diagnostic solutions for detecting infections at their early stages.

CONCLUSIONS

In this work, we developed a glass nanopore device capable of directly sensing amplicons from LAMP native buffer, featuring integrated declogging capabilities and optimized size for qualitative LAMP assay readouts. Our investigation into pore size-dependent LAMP amplicon counting and clogging characteristics revealed that nanopores approximately 200 nm in size offered the best balance between high normalized event rates and reduced clogging frequency. We found that the clogging behavior in low-salt environments differs from the jamming in high-salt conditions due to variations in electrophoretic forces and clogging severity, and simple physical vibration has proven to be an effective solution for resolving clogging in low-salt settings. This success led to the integration of an automated vibration motor into the nanopore device, significantly enhancing its operational lifespan and reliability by reducing downtime and maintenance needs. Applying the system to a Malaria LAMP assay, the clog-free native buffer sensing platform demonstrated a sensitivity of 0.12 parasite/μL, surpassing the detection requirements for identifying infections in asymptomatic individuals. These advancements showcase the potential of our enhanced nanopore device to fulfill the demanding requirements for rapid, reliable, and user-friendly LAMP-based diagnostics. By continuing to refine the vibration-assisted declogging mechanism and enhancing the nanopore device's design and miniaturization, it is feasible to further develop this system into a portable point-of-care device. Such improvements would broaden the scope of nanopore sensing across diverse diagnostic applications. At this stage, our approach enables end point detection of LAMP assay; however, in the future, this platform's capability for extended measurements could enable continuous monitoring throughout the entire LAMP assay amplification process. This

https://doi.org/10.1021/acs.analchem.4c06823
Anal. Chem. 2025, 97, 7879−7887

continuous readout could provide real-time insights into the amplification kinetics and allow for more accurate and dynamic tracking of amplicon formation. Nonetheless, further development is required to address challenges in real-time monitoring. Temperature interference is a major challenge, as the elevated temperatures could impact nanopore stability and cause signal drift. Additionally, current systems have limited data throughput, restricting event detection during real-time reactions. Furthermore, advanced data processing algorithms will also be required to filter noise, correct temperature fluctuations, and analyze the complex data generated. Addressing these issues will be critical for enhancing the platform's capabilities, making it suitable for real-time, on-site diagnostics and broadening its applicability in point-of-care settings.

AUTHOR INFORMATION

Corresponding Author

Weihua Guan − *Department of Electrical Engineering and Department of Biomedical Engineering, Pennsylvania State University, University Park, Pennsylvania 16802, United States; Department of Intelligent Systems Engineering, Luddy School of Informatics, Computing, and Engineering, Indiana University, Bloomington, Indiana 47408, United States;* orcid.org/0000-0002-8435-9672; Email: guanw@iu.edu

Authors

Ming Dong − *Department of Electrical Engineering, Pennsylvania State University, University Park, Pennsylvania 16802, United States;* orcid.org/0000-0002-9071-5717

Aneesh Kshirsagar − *Department of Electrical Engineering, Pennsylvania State University, University Park, Pennsylvania 16802, United States;* orcid.org/0000-0003-2288-5439

Anthony J. Politza − *Department of Biomedical Engineering, Pennsylvania State University, University Park, Pennsylvania 16802, United States;* orcid.org/0009-0005-8670-2357

Muhammad Asad Ullah Khalid − *Department of Electrical Engineering, Pennsylvania State University, University Park, Pennsylvania 16802, United States;* orcid.org/0000-0001-5926-1764

Md Ahasan Ahamed − *Department of Electrical Engineering, Pennsylvania State University, University Park, Pennsylvania 16802, United States*

Complete contact information is available at: https://pubs.acs.org/10.1021/acs.analchem.4c06823

Author Contributions

D.M. performed nanopore experiments. A.K. and A.P. helped develop the LAMP assays. M.A.A. and M.A.K. helped build the nanopore setup. W.G. conceived the concept and supervised the study. W.G. and D.M. cowrote the manuscript and discussed it with all the other authors.

Notes

The authors declare no competing financial interest.

ACKNOWLEDGMENTS

This work was partially supported by the National Science Foundation (2045169, 2319913), National Institutes of Health (R33AI147419), and American Rescue Plan Act through USDA APHIS (Collaborative award# 2023-70432-41395). Any opinions, findings, conclusions, or recommendations expressed in this work are those of the authors and do not necessarily reflect the views of the NSF, NIH and USDA.

REFERENCES

(1) Notomi, T.; Okayama, H.; Masubuchi, H.; Yonekawa, T.; Watanabe, K.; Amino, N.; Hase, T. *Nucleic Acids Res.* **2000**, *28* (12), E63.

(2) Nagamine, K.; Hase, T.; Notomi, T. *Mol. Cell. Probes* **2002**, *16* (3), 223−229.

(3) Mori, Y.; Nagamine, K.; Tomita, N.; Notomi, T. *Biochem. Biophys. Res. Commun.* **2001**, *289* (1), 150−154.

(4) Tomita, N.; Mori, Y.; Kanda, H.; Notomi, T. *Nat. Protoc.* **2008**, *3* (5), 877−882.

(5) Tanner, N. A.; Zhang, Y.; Evans, T. C., Jr. *BioTechniques* **2012**, *53* (2), 81−89.

(6) Xue, L.; Yamazaki, H.; Ren, R.; Wanunu, M.; Ivanov, A. P.; Edel, J. B. *Nat. Rev. Mater.* **2020**, *5* (12), 931−951.

(7) Taxt, A. M.; Avershina, E.; Frye, S. A.; Naseer, U.; Ahmad, R. *Sci. Rep.* **2020**, *10* (1), 7622.

(8) Lee, K.; Park, K.-B.; Kim, H.-J.; Yu, J.-S.; Chae, H.; Kim, H.-M.; Kim, K.-B. *Adv. Mater.* **2018**, *30* (42), No. 1704680.

(9) Freedman, K. J.; Bastian, A. R.; Chaiken, I.; Kim, M. J. *Small* **2013**, *9* (5), 750−759.

(10) Firnkes, M.; Pedone, D.; Knezevic, J.; Döblinger, M.; Rant, U. *Nano Lett.* **2010**, *10* (6), 2162−2167.

(11) Fologea, D.; Uplinger, J.; Thomas, B.; McNabb, D. S.; Li, J. *Nano Lett.* **2005**, *5* (9), 1734−1737.

(12) Pabst, G.; Hodzic, A.; Štrancar, J.; Danner, S.; Rappolt, M.; Laggner, P. *Biophys. J.* **2007**, *93* (8), 2688−2696.

(13) Heinz, C.; Engelhardt, H.; Niederweis, M. *J. Biol. Chem.* **2003**, *278* (10), 8678−8685.

(14) Tang, Z.; Choi, G.; Nouri, R.; Guan, W. *Nano Lett.* **2019**, *19* (11), 7927−7934.

(15) Tang, Z.; Nouri, R.; Dong, M.; Yang, J.; Greene, W.; Zhu, Y.; Yon, M.; Nair, M. S.; Kuchipudi, S. V.; Guan, W. *Biosens. Bioelectron.* **2022**, *197*, No. 113759.

(16) Dong, M.; Kshirsagar, A.; Politza, A. J.; Guan, W. *ACS Nano* **2024**, *18* (9), 7170−7179.

(17) Nouri, R.; Tang, Z.; Guan, W. *ACS Sens.* **2019**, *4* (11), 3007−3013.

(18) He, Y.; Tsutsui, M.; Fan, C.; Taniguchi, M.; Kawai, T. *ACS Nano* **2011**, *5* (7), 5509−5518.

(19) Kirby, B. J.; Hasselbrink, E. F., Jr. *ELECTROPHORESIS* **2004**, *25* (2), 187−202.

(20) Tighe, S. W.; Hayden, A. F.; Kuentzel, M. L.; Eckstrom, K. M.; Foox, J.; Vellone, D. L.; Finstad, K. H.; Laaguiby, P. K.; Hoffman, J. J.; Chittur, S. V. *J. Biomol. Technol. JBT* **2021**, *32* (3), 199−205.

(21) Keller, N.; Grimes, S.; Jardine, P. J.; Smith, D. E. *Nat. Phys.* **2016**, *12* (8), 757−761.

(22) Kurz, V.; Nelson, E. M.; Shim, J.; Timp, G. *ACS Nano* **2013**, *7* (5), 4057−4069.

(23) Ando, G.; Hyun, C.; Li, J.; Mitsui, T. *ACS Nano* **2012**, *6* (11), 10090−10097.

(24) Sim, A. Y. L.; Lipfert, J.; Herschlag, D.; Doniach, S. *Phys. Rev. E* **2012**, *86* (2), No. 021901.

(25) Duleba, D.; Dutta, P.; Denuga, S.; Johnson, R. P. *ACS Meas. Sci. Au* **2022**, *2* (3), 271−277.

(26) Schoch, R. B.; Han, J.; Renaud, P. *Rev. Mod. Phys.* **2008**, *80* (3), 839−883.

(27) Nouri, R.; Tang, Z.; Guan, W. *Anal. Chem.* **2019**, *91* (17), 11178−11184.

(28) Carnerup, A. M.; Ainalem, M.-L.; Alfredsson, V.; Nylander, T. *Soft Matter* **2011**, *7* (2), 760−768.

(29) Burak, Y.; Ariel, G.; Andelman, D. *Biophys. J.* **2003**, *85* (4), 2100−2110.

(30) Shankla, M.; Aksimentiev, A. *Nat. Commun.* **2014**, *5* (1), 5171.

(31) Luan, B.; Aksimentiev, A. *Phys. Rev. E* **2008**, *78* (2), No. 021912.

(32) Saadatmand, M.; Kawaji, M. *Phys. Rev. E* **2013**, *88* (2), No. 023019.
(33) Zhang, P.; Bachman, H.; Ozcelik, A.; Huang, T. J. *Annu. Rev. Anal. Chem.* **2020**, *13* (1), 17−43.
(34) Li, S.; Zeng, S.; Wen, C.; Barbe, L.; Tenje, M.; Zhang, Z.; Hjort, K.; Zhang, S.-L. *J. Phys. Chem. B* **2020**, *124* (51), 11573−11583.
(35) Aksimentiev, A.; Heng, J. B.; Timp, G.; Schulten, K. *Biophys. J.* **2004**, *87* (3), 2086−2097.
(36) Ma, B.; Kim, J.-W.; Tung, S. *IEEE Open J. Nanotechnol.* **2022**, *3*, 124−130.
(37) Belkin, M.; Aksimentiev, A. *ACS Appl. Mater. Interfaces* **2016**, *8* (20), 12599−12608.
(38) Luo, Z.; Sullivan, S. A.; Carlton, J. M. *Ann. N.Y. Acad. Sci.* **2015**, *1342* (1), 53−61.

https://doi.org/10.1021/acs.analchem.4c06823
Anal. Chem. 2025, 97, 7879−7887